

Centrifugo-magnetic pump for gas-to-liquid sampling

Stefan Haeberle^{a,*}, Norbert Schmitt^a, Roland Zengerle^{a,b}, Jens Duerée^{a,b}

^a *Laboratory for MEMS Applications, Department of Microsystems Engineering (IMTEK), University of Freiburg, Georges-Koehler-Allee 106, 79110 Freiburg, Germany*

^b *HSG-IMIT, Institute for Micromachining and Information Technology, Wilhelm-Schickard-Straße 10, 78052 Villingen-Schwenningen, Germany*

Received 28 February 2006; received in revised form 30 August 2006; accepted 6 September 2006
Available online 13 October 2006

Abstract

This paper describes a novel gas micropump realized on a centrifugal microfluidic platform. The pump is integrated on a passive and microstructured polymer disk which is sealed by an elastomer lid featuring paramagnetic inlays. The rotational motion of this hybrid over a stationary magnet induces a designated sequence of volume displacements of the elastic lid, leading to a net transport of gas. The pumping pressure was determined as a function of the frequency of rotation, with a maximum observable pressure of 4.1 kPa without further optimization.

The first application of this rotary device is the production of gas–liquid flows by pumping ambient air into a continuous centrifugal flow of liquid. The injected gas volume segments the liquid stream into a series of liquid compartments. Apart from such multi-phase flows, the new pumping technique supplements a generic air-to-liquid sampling method to centrifugal microfluidic platforms.

© 2006 Elsevier B.V. All rights reserved.

Keywords: Centrifugal microfluidics; Micropump; Segmented flow; Gas–liquid sampling

1. Introduction

The toolbox of centrifugal microfluidics has been continuously extended over the last decade. Up to now, a diverse set of unit operations such as cell-lysis [1], continuous micromixing [2–4], hematocrit determination [5] as well as applications in (bio-)analytics [6,7] and emulsification [8] for micro process engineering have been successfully implemented. However, the processing of gases in rotating microchannels still remains a challenge since the centrifugal field used for pumping scales with the fluid density, thus reducing the force density on gases by three orders of magnitude with respect to liquids. In particular the generation of gas–liquid flows is aggravated by the buoyancy of the gas under the strong “artificial-gravity” conditions of the centrifugal field.

To access the interesting field of gas–liquid flows [9] with our centrifugal platform, the gas has to be additionally pressurized with respect to the liquid. To comply with the modular concept of the rotary system, the typically disposable disk should remain

passive and the force transmission ought to be accomplished in a contact-free fashion. We chose a centrifugo-magnetical principle to displace movable, disk-based steel plates which are incorporated in the lid by permanent magnets aligned along the orbit of the pumping chamber [10].

Several magnetically driven micropumps were presented recently where external electro-magnets deflect permanent magnets integrated on elastic membranes [11–13]. Silicone elastomers, predominantly PDMS, are commonly used due to their simple handling, adjustable elastic properties as well as their cost-efficiency [14,15]. Compared to these approaches, our novel design significantly simplifies the setup by drawing the power for both, the centrifugal liquid pumping as well as the pressurization of the gas, quasi-independently from the same rotary power source. Therefore, no additional power supply is needed to operate the gas-processing part.

The so realized centrifugo-magnetic pumping of gases supplements our recently presented centrifugal platform for continuous liquid-processing [2,8,16]. On this platform, liquid flows are propelled by the pulse-free centrifugal “artificial-gravity” field which is self-stabilized by the inertia associated with the spinning motion. The constant pumping force is of particular benefit for the well-controlled formation of liquid–fluid

* Corresponding author. Tel.: +49 761 203 7476; fax: +49 761 203 7539.
E-mail address: haeberle@imtek.de (S. Haeberle).

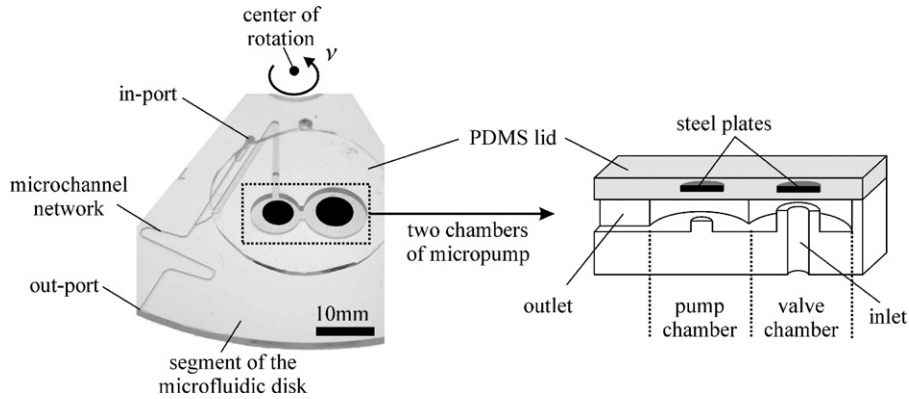


Fig. 1. Sector of the microfluidic disk featuring a network of sealed microchannels. A thin PDMS lid with a thickness of roughly 0.7 mm incorporating two steel plates is placed above the two pump chambers. The disk spins at a frequency ν to pump liquid through the microchannel network (starting from the in-port towards the out-port). In addition, environmental gas is pumped by the sequential displacement of the membrane into the pump chambers while passing a stationary permanent magnet (Fig. 2).

interfaces, e.g. water-in-oil flows, with respect to the reciprocating actuation principles of common mechanical pumps.

This paper starts with an outline of the principle of the centrifugo-magnetic gas pump followed by the device fabrication. Next, we supply the proof of concept and the experimental characterization of the pump. In the last section, the production of gas-liquid flows is presented.

2. Functional principle

Two chambers of our novel, centrifugo-magnetically actuated micropump are located at the same radial but different azimuthal positions. The two chambers are a valve chamber able to seal the gas inlet channel and a pump chamber compressing the gas inside the chamber and the connected channel network at the outlet. The two chambers are sealed by a flexible PDMS lid incorporating metallic inlays (steel, thickness: 400 μm , diameter: 5 mm for the pump and 6 mm for the valve

chamber, respectively). The outlet of the pump is linked to a microfluidic channel network (Fig. 1).

The steel plate inlays above the chambers pass a conventional permanent magnet placed at a fixed position along the orbit of the pump. Its vertical distance is set to approximately 4 mm below the metallic inlays. The magnetic force triggers two phase-shifted displacements in the chambers (Fig. 2).

The pumping sequence exhibits four stages: (a) closing of the valve with the PDMS-membrane at the seat of the valve chamber; (b) compression of the pump chamber to displace a defined gas volume into the connected microchannel via the outlet while the valve is closed; (c) after the permanent magnet has passed the valve chamber, the inlet is opened again; in the last stage (d), the pump chamber is refilled by ambient gas due to the relaxation of the membrane (the magnet has now also passed the pump chamber). During the final step, the small hydrodynamic resistance of the refilling path (via the pump inlet) compared to the connection channel (connecting the pump outlet to the microchannel

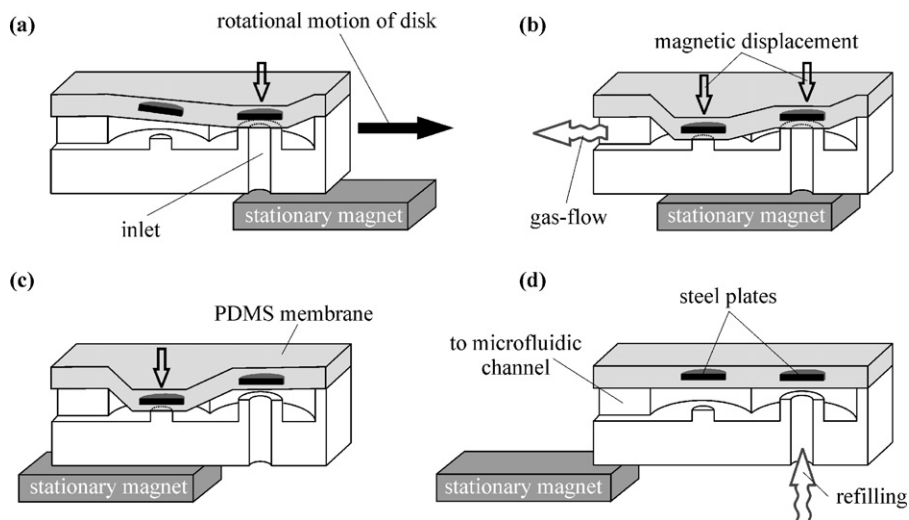


Fig. 2. Functional principle of the gas micropump. The pump chamber orbits above a stationary mounted permanent magnet. The two steel plates within the PDMS lid are spaced at a defined azimuthal distance to induce a sequence of displacements during rotation for pressurizing the gas. After the magnet has passed, the chambers are primarily replenished by ambient gas through the inlet of the valve chamber.

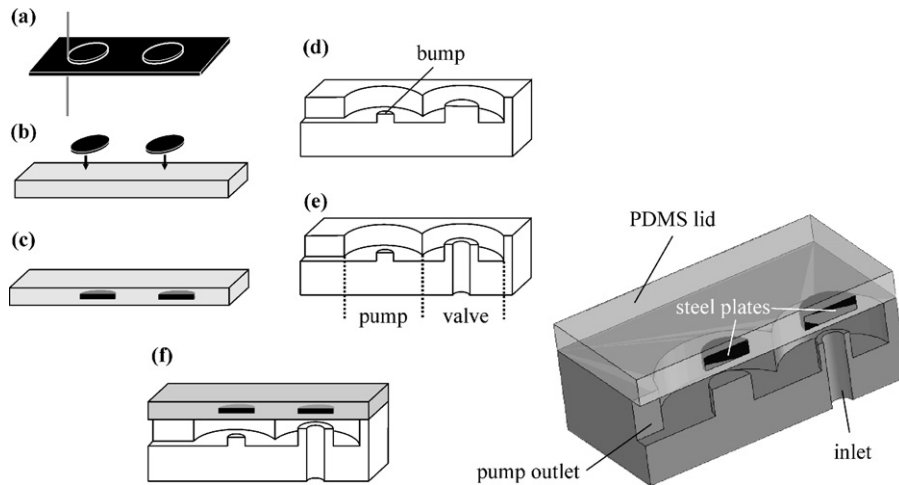


Fig. 3. Fabrication of the passive disk module. Thin, disk-shaped steel plates are cut by electro discharge machining (a), cast into an approximately 0.7 mm thick PDMS lid (b) and bonded by self-adhesion to the microstructured polymer disk (f). The microfluidic structures and pump chambers are fabricated using high-precision milling (d) and drilling processes (e), and partially sealed with an adhesive tape.

network) suppresses backflow from the microchannel connected to the outlet of the pump into the actuation chamber.

The elastomer lid housing the metal inlays constitutes the only moving part of the passive disk while the macroscopic centrifuge periodically actuates the micropump each time the micropump passes the fixed permanent magnet. By arranging more than one magnet along the orbit of the rotating pump, multiple pumping cycles per revolution can be realized.

3. Fabrication

The channels and orifices are micromachined into the polymer substrate by precision engineering processes (Fig. 3). Standard micro milling and drilling processes have been used to fabricate the pump chambers into the polymer. The pump chamber measures a diameter of 8 mm and a depth of 1.2 mm, featuring a bump with a height of 0.7 mm and a diameter of 2.5 mm at its center. This hence corresponds to a maximum displaced stroke volume of $17 \mu\text{L}$ with the maximum stroke of 0.5 mm (membrane hits the bump on the chamber bottom). The valve chamber possesses a diameter of 10 mm and a depth of 1.2 mm, featuring an additional valve seat with a width of 0.3 mm and a distance of 0.2 mm to the membrane around the 2.6-mm diameter inlet. The calculated dead volume of the entire pump (both chambers with closed valve) amounts to $133 \mu\text{L}$.

The microfluidic channel network is (partially) hydrophobically coated and sealed by a transparent adhesive tape to observe the enclosed liquid under rotation at a frequency ν with a stroboscopic measurement setup [17]. The self-adhesive PDMS lid is cast with two integrated steel plates (thickness: $400 \mu\text{m}$, diameter: 5 mm for the pump and 6 mm for the valve chamber, respectively) and cured, resulting in an approximately 0.7-mm thick elastic lid. The steel plates themselves are manufactured by wire electrical discharge machining (WEDM) from standard spring steel. The PDMS lid is aligned above the two chambers which are not sealed with adhesive tape, so that the center of the disk-shaped steel plates matches the bump of the pump and the

inlet of the valve chamber, respectively. Afterwards, the lid is bonded to the disk-surface by adhesion.

4. Pump characteristics

For all the experiments, the disk is mounted up-side down on a centrifugal drive so that the permanent magnet (NdFeB, $25 \text{ mm} \times 12.5 \text{ mm} \times 3 \text{ mm}$, J54-307, Edmund Industrie Optik GmbH) can be positioned along the pump orbit (radial position: 35 mm) at a distance of approximately 2 mm to the disk. This alignment leads to a magnetic field strength of approximately 240 mT directed in the plane of the steel plates when the plate is positioned directly underneath the magnet. With this configuration, the pump generates a pressure pulse within the microfluidic channel network connected to the outlet of the pump during 4.6 ms at a rotational frequency of 10 Hz (see Fig. 4).

4.1. Proof of principle

The functional principle of the micropump is directly visualized by the displacement of an ink-colored liquid plug through a meander-shaped microchannel (Fig. 5). Within the azimuthal

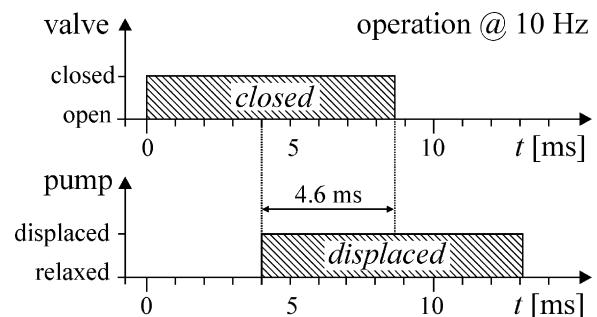


Fig. 4. Timeline of one actuation cycle of the pump at a rotational frequency of 10 Hz. A full revolution takes 100 ms. The membrane of the valve and pump chamber, respectively, are considered to be deflected as soon as the complete steel plates have entered the magnetic field (dimensions of magnet).

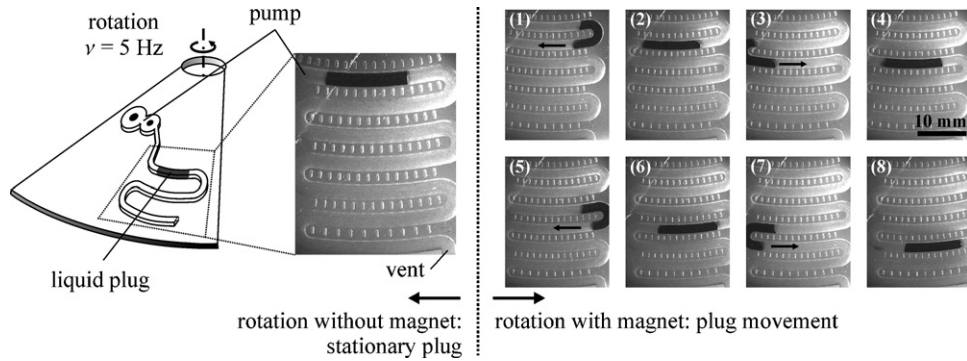


Fig. 5. In this proof-of-principle investigation, the outlet of the micropump is connected to a meander-shaped channel. The stroboscopic picture in the middle shows a static ink-colored liquid plug within the microchannel while rotating at 5 Hz without a magnet placed along the pump orbit. (1–8) As soon as the permanent magnet is placed at the orbit of the pump, the pump is “on” to suck in environmental air and thus displace the plug in a stepwise fashion through the meander.

channel parts, the plug is merely actuated by the micropump, only, as no net centrifugal force applies. A static liquid plug (colored with ink for visualization) can be observed without a magnet at the pump orbit. A periodic and steady forward motion of the plug initiates as soon as the stationary permanent magnet is placed at the orbit of the pump. This proves that the pump periodically introduces a unidirectional gas flow (at vanishing counter pressure) of ambient air into the channels on the disk.

4.2. Counter pressure

A series of experiments was conducted to visualize the maximum pressure head of the gas pump. To this end, the pump is connected to the left arm of the U-shaped channel (width: 1 mm, depth: 500 μm) in Fig. 6. A plug of ink-colored DI-water is introduced into the channel through the right arm that remains open, thus acting as an air vent. Upon rotation, the two liquid–air interfaces of the water plug tend to level out by the principle of hydrostatic pressure balance within the strong centrifugal field of “artificial-gravity” ($\sim 100\text{ g}$ at 30 Hz).

Once the permanent magnet is positioned above the micropump, the air volume in the left arm is exposed to the pumping

pressure p while the air in the right arm remains at the ambient pressure due to the vent. This leads to a radial offset Δr between the opposing menisci of the plug. The asymmetry stabilizes under the impact of the pumping pressure p and the counteracting centrifugal force F_v , and the static equilibrium of Δr represents a direct measure for the maximum achievable back-pressure that results in a zero net-flow.

This pressure can be derived from the equation

$$p = \rho \omega^2 \Delta r \bar{r} \quad (1)$$

with the liquid density ρ , the angular velocity $\omega = 2\pi\nu$ and the mean radial position of the water plug \bar{r} . The results of these measurements are depicted in Fig. 4 (right). For low frequencies of rotation $\nu < 33\text{ Hz}$, the pumping pressure increases almost linearly with the frequency ν up to about 4.1 kPa. Beyond $\nu = 33\text{ Hz}$, the symmetric centrifugal force $F_v \sim \nu^2$ tends to level off Δr , thus limiting the observable range of pumping pressures p since the optical readout of Δr from the stroboscopic gray-scale images is limited to approximately $\pm 0.4\text{ mm}$. At frequencies below 10 Hz, the meniscus in the right arm lifts the plug through the air vent.

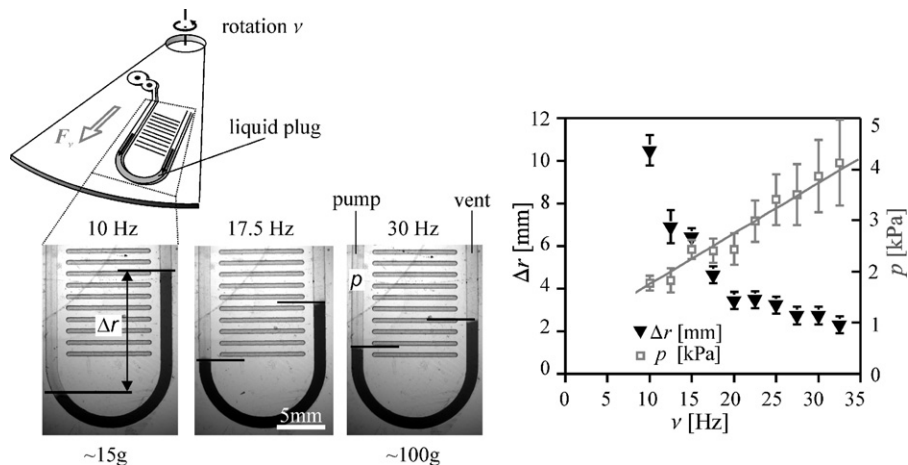


Fig. 6. Visualization of the pressure head by a U-shaped channel (width: 1 mm, depth: 500 μm). Depending on the frequency of rotation ν , a radial offset Δr emerges between the opposing capillaries representing the maximum pressure of the gas micropump. While the pressure head p rises with ν , Δr still tends to vanish towards large ν due to the increasing impact of the radially symmetric centrifugal force F_v (right graph). And since the optical readout of the radial offset is limited to an accuracy of approximately $\pm 0.4\text{ mm}$, our principle of measuring p via Δr is thus confined to the frequency range below about 30 Hz.

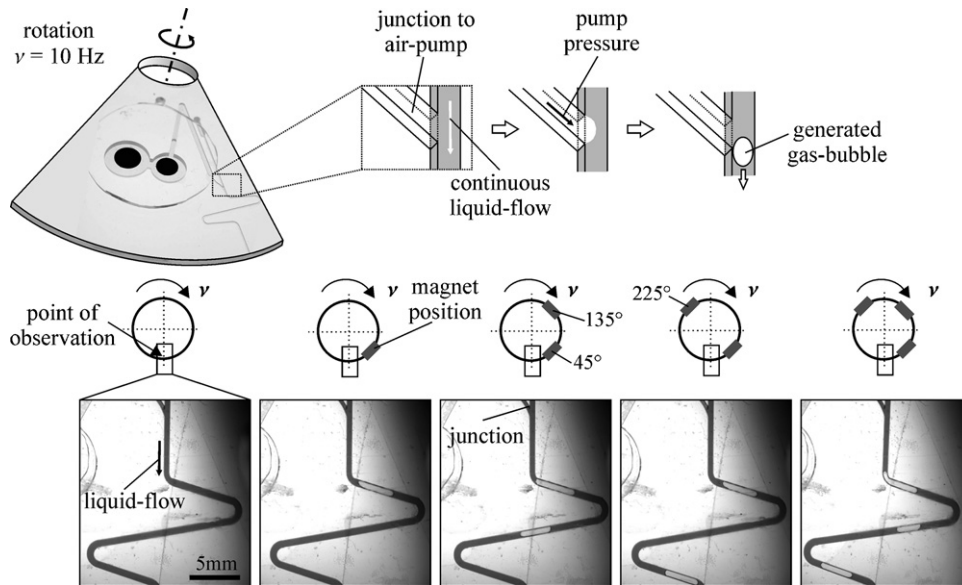


Fig. 7. Different modes of gas–liquid flow at a rotational frequency of $\nu = 10$ Hz within a meander-shaped microchannel (width: $700 \mu\text{m}$, depth: $200 \mu\text{m}$). A segment of the microfluidic disk as well as the principle of the introduction of gas bubbles is shown in the top sketch. The azimuthal positions of the magnets with respect to the camera window are indicated on top of each photograph. The production rate of the gas bubbles depends on the number and the alignment of the permanent magnets along the orbit of the rotating micropump. Without any magnets, no gas bubbles are generated, thus validating the functional principle to the centrifugo-magnetic pump.

The increase of the pumping pressure with the frequency of rotation ν is attributed to the growing number of volume displacement cycles per unit time when a constant stroke is assumed. This frequency dependent effect tends to elevate the average pressure within the pump and thus also in the U-shaped measurement structure.

5. Gas–liquid flow

Fig. 7 visualizes how the pumping pressure can be harnessed for injecting ambient air into a continuous, centrifugally driven liquid stream (ink-colored water). The rotating pump generates a periodic sequence of pressure pulses. Once the gas pressure is sufficiently high at the junction of the outlet channel to the liquid guiding flow channel, a gas bubble is injected into the continuous liquid stream as depicted in the schematic drawing at the top of Fig. 7. At a given frequency of rotation $\nu = 10$ Hz, the bubble rate changes with the number and the azimuthal position(s) of the permanent magnets which can be placed at 45° , 135° and 225° with respect to the point of observation. The number of magnets and the frequency ν also set the volume ratio between gas and liquid phase.

The bubbles within the meander channel display a volume of approximately $0.5 \mu\text{L}$. This is far below the theoretical stroke volume of the pump chamber of $17 \mu\text{L}$ which is displaced by the pumping action. As the overall pressurized volume $139.7 \mu\text{L}$ (volumes of the pump chamber: $133 \mu\text{L}$ plus the volume of the connection channel between the outlet of the pump and the junction: $6.7 \mu\text{L}$) exceeds the inserted volume ($0.5 \mu\text{L}$) by more than a factor of 200, only a small fraction ($<3\%$) of the displaced volume ($<17 \mu\text{L}$) is actually inserted into the liquid.

Assuming a full stroke and neglecting the additional hydrostatic pressure on the bubble as well as backward flow through the valve, the pressure for the insertion hence increases by a factor of about $1.13 = 139.7 \mu\text{L} / (139.7 \mu\text{L} - 17 \mu\text{L} + 0.5 \mu\text{L})$, only, with respect to the undeflected pump membrane. The maximum rate of bubble injection amounts to 30 bubbles per second (with three magnets on the orbit of the pump at $\nu = 10$ Hz). This rate thus corresponds to a gas-injection “flow rate” of $15 \mu\text{L s}^{-1}$ if the volumes are measured under the pressure conditions within the liquid stream and $17 \mu\text{L s}^{-1}$ ($\approx 1.13 \times 15 \mu\text{L s}^{-1}$) measured at ambient pressure.

One easily recognizes that the pump is far away from being optimized regarding the pumping performance. Still, it clearly fulfils our original objective to inject a train of bubbles composed of ambient air into the centrifugal flow through the radial channel.

6. Summary and outlook

We presented for the first time a centrifugo-magnetically actuated gas micropump. Pumping is implemented by the phase-shifted displacement of two metal inlays incorporated in the elastic lid of the passive and possibly disposable polymer disk. The new functional principle as well as the fabrication method well comply with the modular approach of centrifugal microfluidic platforms.

The new pump adds two important unit operations to centrifugally driven microfluidics, the sampling of gas volumes and their introduction to liquid-phase assays on a lab-on-a-disk as well as the generation of trains of discrete liquid plugs segmented by gas bubbles.

Acknowledgements

The authors would like to thank Dr. Ralf Förster from the IMTEK Laboratory for process technology who conducted the WEDM machining, as well as Gerhard Jobst for the micromachining of the polymer substrates.

References

- [1] J. Kim, S.H. Jang, G.Y. Jia, J.V. Zoval, N.A. Da Silva, M.J. Madou, Cell lysis on a microfluidic CD (compact disc), *Lab on a Chip* 4 (2004) 516–522.
- [2] S. Haeberle, T. Brenner, H.P. Schlosser, R. Zengerle, J. Duce, Centrifugal micromixer, *Chem. Eng. Technol.* 28 (2005) 613–616.
- [3] J. Duce, S. Haeberle, T. Brenner, T. Glatzel, R. Zengerle, Patterning of flow and mixing in rotating radial microchannels, *Microfluidics Nanofluidics* 2 (2005) 97–105.
- [4] J. Duce, T. Brenner, S. Haeberle, T. Glatzel, R. Zengerle, Multilamination of flows in planar networks of rotating microchannels, *Microfluidics Nanofluidics* 2 (2006) 78–84.
- [5] L. Riegger, M. Grumann, T. Brefka, J. Steigert, C.P. Steinert, T. Brenner, R. Zengerle, J. Duce, Bubble-free priming of blind capillaries for high-accuracy centrifugal hematocrit measurements, in: *Proceedings of 9th International Conference on Miniaturized Systems for Chemistry and Life Science (μ TAS 2005)*, Boston, USA, 2005, pp. 796–798.
- [6] M. Madou, G. Kellog, LabCD: a centrifuge-based microfluidic platform for diagnostics, in: *Proceedings of SPIE*, 1998, pp. 80–93.
- [7] G. Ekstrand, C. Holmquist, A.E. Örlfors, B. Hellman, A. Larsson, P. Andersson, Microfluidics in a rotating CD, in: *Proceedings of Micro Total Analysis Systems*, 2000, pp. 311–314.
- [8] S. Haeberle, R. Zengerle, J. Duce, Monodisperse droplet trains and segmented flow for centrifugal microfluidics, in: *Proceedings of 9th International Conference on Miniaturized Systems for Chemistry and Life Sciences (μ TAS 2005)*, Boston, USA, 2005, pp. 635–637.
- [9] A. Gunther, M. Jhunjhunwala, M. Thalmann, M.A. Schmidt, K.F. Jensen, Micromixing of miscible liquids in segmented gas–liquid flow, *Langmuir* 21 (2005) 1547–1555.
- [10] M. Grumann, A. Geipel, L. Riegger, R. Zengerle, J. Duce, Batch-mode mixing on centrifugal microfluidic platforms, *Lab on a Chip* 5 (2005) 560–565.
- [11] C. Yamahata, C. Lotto, E. Al-Assaf, M.A.M. Gijs, A PMMA valveless micropump using electromagnetic actuation, *Microfluidics Nanofluidics* 1 (2005) 197–207.
- [12] T.R. Pan, S.J. McDonald, E.M. Kai, B. Ziaie, A magnetically driven PDMS micropump with ball check-valves, *J. Micromech. Microeng.* 15 (2005) 1021–1026.
- [13] C. Yamahata, F. Lacharme, Y. Burri, M.A.M. Gijs, A ball valve micropump in glass fabricated by powder blasting, *Sens. Actuators B-Chem.* 110 (2005) 1–7.
- [14] J. Goulpeau, D. Trouchet, A. Ajdari, P. Tabeling, Experimental study and modeling of polydimethylsiloxane peristaltic micropumps, *J. Appl. Phys.* 98 (2005).
- [15] M.A. Unger, H.P. Chou, T. Thorsen, A. Scherer, S.R. Quake, Monolithic microfabricated valves and pumps by multilayer soft lithography, *Science* 288 (2000) 113–116.
- [16] S. Haeberle, N. Schmitt, R. Zengerle, J. Duce, A centrifuge-magnetically actuated gas micropump, in: *Proceedings of 19th International Conference on Micro Electro Mechanical Systems (MEMS 2006)*, Istanbul, Turkey, 2006, pp. 166–169.
- [17] M. Grumann, T. Brenner, C. Beer, R. Zengerle, J. Duce, Visualization of flow patterning in high-speed centrifugal microfluidics, *Rev. Sci. Instrum.* 76 (2005) 025101.